International Journal of Recent Engineering Research and Development (IJRERD)
ISSN: 2455-8761
www.ijrerd.com || Volume 04 – Issue 09 || September 2019 || PP. 44-53

Dynamics analysis and simulation of the 3-PRS ankle rehabilitation robot

***Zhaungzhuang Mao[1]**

Mengchao Liu[2]

Pengcheng Yang[3]

[1,2,3]School of Mechanical and Power Engineering
Henan Polytechnic University, 454003, Jiaozuo, China
** Corresponding author*

Abstract: Aiming at the complex multi-body dynamic system of the 3-PRS ankle rehabilitation robot parallel mechanism, the dynamic model of the parallel mechanism is solved by Lagrange method, and the dynamic simulation is carried out. Based on the 3D model of the 3-PRS ankle rehabilitation robot, a virtual prototype is constructed, and the simulation examples of kinematics and dynamics of the mechanism are given. The simulation results are compared with those obtained by theoretical analysis, and the correctness of the theoretical analysis is clarified. It lays a solid foundation for the design of the 3-PRS ankle rehabilitation robot and the research of the parallel mechanism.

Keywords: Parallel mechanism, Ankle rehabilitation robot, Inverse kinematic analysis, Dynamic analysis, Virtual prototype

1. Introduction

As a parallel mechanism [1], the ankle rehabilitation robot not only needs to meet the needs of different applications, but also needs to realize the complex action of the ankle joint rehabilitation. Due to the advantages of the parallel mechanism such as low inertia, high stiffness and closed structure [2], devices with parallel mechanism are widely used in many fields. Such as, aerospace, precision machinery manufacture, medical equipment and other fields have many applications [3-7]. Not all ankle rehabilitation robots have 6 degrees-of-freedom (DOFs), so 3-DOFs parallel mechanism and 4-DOFs parallel mechanism are proposed [8]. As a representative of the parallel mechanism, the 3-PRS ankle rehabilitation robot has two rotation DOFs, which can complete the most important ankle rehabilitation movements, namely plantar flexion/dorsiflexion and varus/eversion. The robot also has a translational DOF, according to which the height of the patient on the chair can be adjusted to make it adaptive in the vertical direction. The 3-PRS ankle rehabilitation robot is composed of flexible and rigid objects, so it has complex multi-body dynamics. And it is difficult to analyze the kinematics and dynamics of the parallel mechanism because of its complex motion process. The simulation of dynamics and kinematics of the mechanism is helpful to the analysis of complex parallel mechanism, and the reliability of simulation can be obtained by comparing the simulation value with the theoretical value. In addition, in order to save time and cost, the virtual prototype of the 3-PRS ankle rehabilitation robot is established, because the

virtual prototype technology can reduce the research cost and short the research cycle.

2. Establishment the 3-PRS ankle rehabilitation robot model

The 3-PRS parallel mechanism is composed of three sliding rails fixed on a fixing platform, three sliding blocks, three connecting rods and a moving platform [9-11]. Three ball screw rods (namely slide rails) are evenly distributed at 120 degrees on the fixing platform. Three servo motors at the top drive the slider up and down respectively. A cylindrical hinge is mounted on the three sliding blocks respectively. Three equally long connecting rods are connected to cylindrical hinge and spherical hinge respectively. The rehabilitation robot uses the servo motor as the power input to control the slider motion and determine the posture of the robot moving platform。

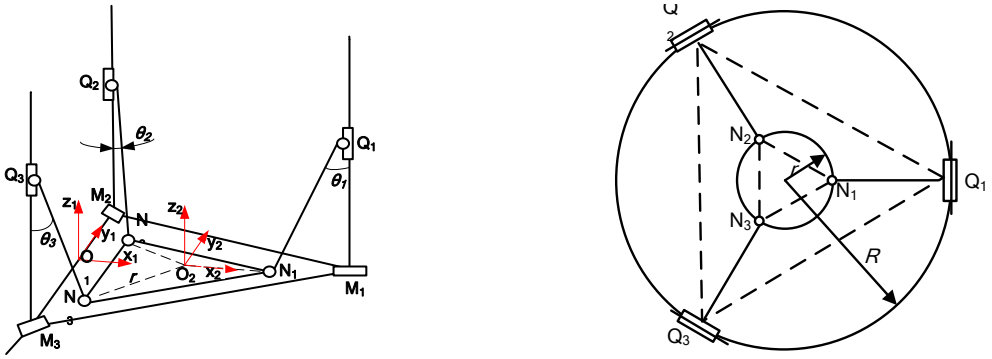

Figure 1: Structural sketch of 3-PRS ankle rehabilitation robot

$M_iQ_iN_i$ $(i=1,2,3)$ are the branch chains, M_i are the vertexes on the base of the mechanism with radius R, and N_i are the vertexes on the moving platform with radius r. Q_iN_i are the length of the connecting rods and denoted as L_i, and M_iQ_i are the distance between the sliders and the fixed platform, denoted as H_i. θ_i are the Angle between Q_iN_i and M_iQ_i.

According to Figure 1, the fixing coordinate system O_1-xyz and the moving coordinate system O_2-xyz are established, and denoted as G and D respectively. The angle at which D rotates around the z axis of G is denoted by γ, the rotation angle about the y axis is denoted by β, and the rotation angle about the x axis is denoted by α. The component of the O_2 with respect to the positional parameter of O_1 on the x axis is denoted by x_t, the component on the y axis is denoted by y_t, and the component on the z axis is denoted by z_t. The homogeneous transformation matrix of D relative to G can be expressed as

$$T=\begin{bmatrix} \cos\beta\cos\gamma & -\cos\beta\sin\gamma & \sin\beta & x_t \\ \cos\alpha\sin\gamma-\sin\alpha\sin\beta\cos\gamma & \cos\alpha\cos\gamma-\sin\alpha\sin\beta\sin\gamma & -\sin\alpha\cos\beta & y_t \\ \sin\alpha\sin\gamma-\cos\alpha\,s\,\beta\cos\gamma & \sin\alpha\cos\gamma+\cos\alpha\sin\beta\sin\gamma & \cos\alpha\cos\beta & z_t \\ 0 & 0 & 0 & 1 \end{bmatrix} \quad (1)$$

3. Dynamic analysis

Dynamic analysis of the parallel robot [12-13] is to study the relationship between mechanical forces and motion parameters in the movement process. Due to constraints and closed chain structure, the dynamic model of the parallel mechanism is more complex than that of series mechanism, which belongs to multi-body dynamic system. At present, Kane, Newton-Euler and Lagrange are commonly used.

In the paper, Lagrange is adopted for dynamic analysis of the 3-PRS ankle rehabilitation robot. Lagrange equation can be expressed as

$$\begin{cases} \dfrac{d}{dt}\left(\dfrac{\partial L}{\partial \dot{q}_i}\right)-\dfrac{\partial L}{\partial q_i}=Q_i \quad (i=1,2,3) \\ L=T-V \end{cases} \tag{2}$$

where L is the Lagrange function, T and V are the kinetic energy and potential energy respectively, q_i and Q_i are the generalized forces and generalized coordinates of the system respectively, i is the system DOFs.

The point N_i on the moving platform can be expressed as $\left(X'_{N1}\ Y'_{N1}\ Z'_{N1}\right)^{\mathrm{T}}$ in O_2-xyz. According to the mechanism size expression of the point N_i in the three branch chains and the transformation matrix expression are equal, which can be expressed as

$$\begin{cases} X'_{Ni}\ k_1+Y'_{Ni}\ m_1+Z'_{Ni}\ n_1+x_t=K(i)\left(X_{Mi}-\dfrac{1}{2}L_i\sin\theta_i\right) \\ X'_{Ni}k_2+Y'_{Ni}m_2+Z'_{Ni}\ n_2+y_t=K'(i)\left(Y_{Mi}-\dfrac{\sqrt{3}}{2}L_i\sin\theta_i\right) \\ X'_{Ni}k_3+Y'_{Ni}m_3+Z'_{Ni}\ n_3+z_t=H_i-L_i\cos\theta_i \end{cases} \tag{3}$$

$$K(i)=\begin{cases} 1 & (i=1) \\ -1 & (i=2,3) \end{cases} \qquad K'(i)=\begin{cases} 1 & (i=1,2) \\ -1 & (i=3) \end{cases} \tag{4}$$

$$\begin{cases} \theta_1=\arcsin\dfrac{\left|X_{N1}-X_{M1}\right|}{L_1} \\ \theta_2=\arcsin\dfrac{\left|2X_{N2}\right|}{L_2} \\ \theta_3=\arcsin\dfrac{\left|2X_{N3}\right|}{L_3} \end{cases} \tag{5}$$

In the fixed coordinate system O_1-xyz, the quality of sliders $\mathrm{Q}_i\ (i=1,2,3)$ are denoted as m_i, Since the centroid is on the slide track, the centroid of connecting rods $\mathrm{Q}_i\mathrm{N}_i$ can be denoted as $\left(X_{ci}\ \ Y_{ci}\ \ Z_{ci}\right)^{\mathrm{T}}$, and can be expressed as

$$\begin{cases} X_{c1}=\dfrac{3}{2}R-\dfrac{1}{2}L_1\sin\theta_1 \\ Y_{c1}=0 \\ Z_{c1}=H_1-\dfrac{1}{2}L_1\cos\theta_1 \end{cases} \tag{6}$$

$$\begin{cases} X_{c2} = \dfrac{1}{4} L_2 \sin\theta_2 \\ Y_{c2} = \dfrac{\sqrt{3}}{2}\left(R - L_2 \sin\theta_2\right) + \dfrac{\sqrt{3}}{4} L_2 \sin\theta_2 \\ Z_{c2} = H_2 - \dfrac{1}{2} L_2 \cos\theta_2 \end{cases} \tag{7}$$

$$\begin{cases} X_{c3} = \dfrac{1}{4} L_3 \sin\theta_3 \\ Y_{c3} = -\dfrac{\sqrt{3}}{2}\left(R - L_3 \sin\theta_3\right) - \dfrac{\sqrt{3}}{4} L_3 \sin\theta_3 \\ Z_{c3} = H_3 - \dfrac{1}{2} L_3 \cos\theta_3 \end{cases} \tag{8}$$

The quality of connecting rods Q_iN_i are denoted as m_{Li}, the centroid velocity is $\left(\dot{X}_{ci} \quad \dot{Y}_{ci} \quad \dot{Z}_{ci}\right)^{\mathrm{T}}$, and the rotational inertia about the centroid in the axis direction of the rotating pair is J_i. The quality of platform $N_1N_2N_3$ is denoted as m_{N}, the centroid is O_2, the displacement velocity and angular velocity relative to the fixed coordinate system O_1-xyz are $\mathbf{V}_{\mathrm{N}} = \left(\dot{x}_t \quad \dot{y}_t \quad \dot{z}_t\right)^{\mathrm{T}}$ and $\boldsymbol{\omega}_N = \left(\dot{\alpha} \quad \dot{\beta} \quad \dot{\gamma}\right)^{\mathrm{T}}$ respectively, and the inertia matrix around the centroid is $\mathbf{J}_{\mathrm{N}}$. The plane of base $M_1M_2M_3$ is used as the horizontal plane, and the dynamic model is simplified by ignoring the connection friction. The actual inertia matrix of $N_1N_2N_3$ platform can be expressed as

$$\mathbf{J}_{\mathrm{N}} = \begin{bmatrix} J_x & 0 & 0 \\ 0 & J_y & 0 \\ 0 & 0 & J_z \end{bmatrix} \tag{9}$$

The gravitational acceleration is denoted as g, the time as t, and the kinetic energy T and potential energy V of the mechanism can be expressed as

$$T = \frac{1}{2}\sum_{i=1}^{3}\left[m_i\left(\dot{X}_{ci}^{\,2} + \dot{Y}_{ci}^{\,2} + \dot{Z}_{ci}^{\,2}\right) + m_{hi}\dot{H}_i^{\,2} + J_i\dot{\theta}_i^{\,2}\right] + \frac{1}{2} m_N \mathbf{V}_N^{\,T}\mathbf{V}_N + \frac{1}{2}\boldsymbol{\omega}_N^{\,T}\mathbf{J}_N\boldsymbol{\omega}_N \tag{10}$$

$$V = \sum_{i=1}^{3}\left(m_{hi} g H_i + m_i g Z_{ci}\right) + m_N g x_t \tag{11}$$

By deriving Equations (6), (7) and (8) with respect to time t, the outcomes are obtained. The outcomes are substituted into Equation (10), which can be expressed as

$$T = \frac{1}{2}\left(\hat{m}_{11}\dot{H}_1^{\,2} + \hat{m}_{22}\dot{H}_2^{\,2} + \hat{m}_{33}\dot{H}_3^{\,2}\right) + \hat{m}_{12}\dot{H}_1\dot{H}_2 + \hat{m}_{13}\dot{H}_1\dot{H}_3 + \hat{m}_{23}\dot{H}_2\dot{H}_3 \tag{12}$$

where,

$$\begin{aligned} \hat{m}_{11} = {} & m_{h1} + m_1\left(1 + L_1 \sin\theta_1 A_1\right) + \left(J_1 + \frac{1}{4} m_1 L_1^{\,2}\right) A_1^{\,2} + \left(J_2 + \frac{1}{4} m_2 L_2^{\,2}\right) B_1^{\,2} \\ & + \left(J_3 + \frac{1}{4} m_3 L_3^{\,2}\right) C_1^{\,2} + m_{\mathrm{N}}\left(D_1^{\,2} + E_1^{\,2} + F_1^{\,2}\right) + J_x G_1^{\,2} + J_y M_1^{\,2} + J_z N_1^{\,2} \end{aligned} \tag{13}$$

$$\begin{aligned} \hat{m}_{22} = {} & m_{h2} + m_2\left(1 + L_2 \sin\theta_2 B_2\right) + \left(J_1 + \frac{1}{4} m_1 L_1^{\,2}\right) A_2^{\,2} + \left(J_2 + \frac{1}{4} m_2 L_2^{\,2}\right) B_2^{\,2} \\ & + \left(J_3 + \frac{1}{4} m_3 L_3^{\,2}\right) C_2^{\,2} + m_{\mathrm{N}}\left(D_2^{\,2} + E_2^{\,2} + F_2^{\,2}\right) + J_x G_2^{\,2} + J_y M_2^{\,2} + J_z N_2^{\,2} \end{aligned} \tag{14}$$

$$\hat{m}_{33} = m_{h3} + m_3\left(1 + L_3 \sin\theta_3 C_3\right) + \left(J_1 + \frac{1}{4}m_1 L_1^{\,2}\right)A_3^{\,2} + \left(J_2 + \frac{1}{4}m_2 L_2^{\,2}\right)B_3^{\,2} + \left(J_3 + \frac{1}{4}m_3 L_3^{\,2}\right)C_3^{\,2} + m_{\mathrm{N}}\left(D_3^{\,2} + E_3^{\,2} + F_3^{\,2}\right) + J_x G_3^{\,2} + J_y M_3^{\,2} + J_z N_3^{\,2} \tag{15}$$

$$\hat{m}_{12} = \left(J_1 + \frac{1}{4}m_1 L_1^{\,2}\right)A_1 A_2 + \left(J_2 + \frac{1}{4}m_2 L_2^{\,2}\right)B_1 B_2 + \left(J_3 + \frac{1}{4}m_3 L_3^{\,2}\right)C_1 C_2 + \frac{1}{2}m_1 L_1 \sin\theta_1 A_2 + \frac{1}{2}m_2 L_2 \sin\theta_2 B_1 + m_{\mathrm{N}}\left(D_1 D_2 + E_1 E_2 + F_1 F_2\right) + J_x G_1 G_2 + J_y M_1 M_2 + J_z N_1 N_2 \tag{16}$$

$$\hat{m}_{13} = \left(J_1 + \frac{1}{4}m_1 L_1^{\,2}\right)A_1 A_3 + \left(J_2 + \frac{1}{4}m_2 L_2^{\,2}\right)B_1 B_3 + \left(J_3 + \frac{1}{4}m_3 L_3^{\,2}\right)C_1 C_3 + \frac{1}{2}m_1 L_1 \sin\theta_1 A_3 + \frac{1}{2}m_3 L_3 \sin\theta_3 C_1 + m_{\mathrm{N}}\left(D_1 D_3 + E_1 E_3 + F_1 F_3\right) + J_x G_1 G_3 + J_y M_1 M_3 + J_z N_1 N_3 \tag{17}$$

$$\hat{m}_{23} = \left(J_1 + \frac{1}{4}m_1 L_1^{\,2}\right)A_2 A_3 + \left(J_2 + \frac{1}{4}m_2 L_2^{\,2}\right)B_2 B_3 + \left(J_3 + \frac{1}{4}m_3 L_3^{\,2}\right)C_2 C_3 + \frac{1}{2}m_2 L_2 \sin\theta_2 B_3 + \frac{1}{2}m_3 L_3 \sin\theta_3 C_2 + m_{\mathrm{N}}\left(D_2 D_3 + E_2 E_3 + F_2 F_3\right) + J_x G_2 G_3 + J_y M_2 M_3 + J_z N_2 N_3 \tag{18}$$

where，

$$A_i = \frac{\partial\theta_1}{\partial H_i} \quad B_i = \frac{\partial\theta_2}{\partial H_i} \quad C_i = \frac{\partial\theta_3}{\partial H_i} \quad D_i = \frac{\partial x_t^T}{\partial H_i} \quad E_i = \frac{\partial y_t^T}{\partial H_i}$$
$$F_i = \frac{\partial z_t^T}{\partial H_i} \quad G_i = \frac{\partial\alpha}{\partial H_i} \quad M_i = \frac{\partial\beta}{\partial H_i} \quad N_i = \frac{\partial\gamma}{\partial H_i} \quad (i = 1,2,3) \tag{19}$$

$\hat{m}_{11}$, $\hat{m}_{22}$, $\hat{m}_{33}$, $\hat{m}_{12}$, $\hat{m}_{13}$ and $\hat{m}_{23}$ are set as the equivalent mass, $\dot{H}_1$, $\dot{H}_2$ and $\dot{H}_3$ are the velocity of generalized coordinates, and F_1, F_2 and F_3 are the generalized force of the system.

By deriving Equation (3) with respect to the generalized coordinates H_1, H_2 and H_3 respectively, the parameter values A_i, B_i, C_i, D_i, E_i, F_i, G_i, M_i and N_i are obtained. Therefore, the Lagrange equation can be expressed as

$$\frac{\mathrm{d}}{\mathrm{d}t}\left(\frac{\partial T}{\partial \dot{H}_i}\right) - \frac{\partial T}{\partial H_i} + \frac{\partial V}{\partial H_i} = F_i \tag{20}$$

Equation (20) can be simplified as

$$F_1 = \hat{m}_{11}\ddot{H}_1 + \hat{m}_{12}\ddot{H}_2 + \hat{m}_{13}\ddot{H}_3 + \frac{1}{2}\frac{\partial\hat{m}_{11}}{\partial H_1}\dot{H}_1^{\,2} + \frac{\partial\hat{m}_{11}}{\partial H_2}\dot{H}_1\dot{H}_2 + \left(\frac{\partial\hat{m}_{12}}{\partial H_2} - \frac{1}{2}\frac{\partial\hat{m}_{22}}{\partial H_1}\right)\dot{H}_2^{\,2} + \left(\frac{\partial\hat{m}_{13}}{\partial H_3} - \frac{1}{2}\frac{\partial\hat{m}_{33}}{\partial H_1}\right)\dot{H}_3^{\,2} + \frac{\partial\hat{m}_{11}}{\partial H_3}\dot{H}_1\dot{H}_3 + \left(\frac{\partial\hat{m}_{12}}{\partial H_3} + \frac{\partial\hat{m}_{13}}{\partial H_2} - \frac{\partial\hat{m}_{23}}{\partial H_1}\right)\dot{H}_2\dot{H}_3 + \frac{\partial V}{\partial H_1} \tag{21}$$

$$F_2 = \hat{m}_{12}\ddot{H}_1 + \hat{m}_{22}\ddot{H}_2 + \hat{m}_{23}\ddot{H}_3 + \frac{1}{2}\frac{\partial\hat{m}_{22}}{\partial H_2}\dot{H}_2^{\,2} + \frac{\partial\hat{m}_{22}}{\partial H_1}\dot{H}_1\dot{H}_2 + \left(\frac{\partial\hat{m}_{23}}{\partial H_3} - \frac{1}{2}\frac{\partial\hat{m}_{33}}{\partial H_2}\right)\dot{H}_3^{\,2} + \left(\frac{\partial\hat{m}_{12}}{\partial H_1} - \frac{1}{2}\frac{\partial\hat{m}_{11}}{\partial H_2}\right)\dot{H}_1^{\,2} + \frac{\partial\hat{m}_{22}}{\partial H_3}\dot{H}_2\dot{H}_3 + \left(\frac{\partial\hat{m}_{12}}{\partial H_3} - \frac{\partial\hat{m}_{13}}{\partial H_2} + \frac{\partial\hat{m}_{23}}{\partial H_1}\right)\dot{H}_1\dot{H}_3 + \frac{\partial V}{\partial H_2} \tag{22}$$

$$F_3 = \hat{m}_{13}\ddot{H}_1 + \hat{m}_{23}\ddot{H}_2 + \hat{m}_{33}\ddot{H}_3 + \frac{1}{2}\frac{\partial \hat{m}_{33}}{\partial H_3}\dot{H}_3^{\,2} + \frac{\partial \hat{m}_{33}}{\partial H_1}\dot{H}_1\dot{H}_3 + \left(\frac{\partial \hat{m}_{13}}{\partial H_1} - \frac{1}{2}\frac{\partial \hat{m}_{11}}{\partial H_3}\right)\dot{H}_1^{\,2}$$
$$+\left(\frac{\partial \hat{m}_{23}}{\partial H_2} - \frac{1}{2}\frac{\partial \hat{m}_{22}}{\partial H_3}\right)\dot{H}_2^{\,2} + \frac{\partial \hat{m}_{33}}{\partial H_2}\dot{H}_2\dot{H}_3 + \left(\frac{\partial \hat{m}_{23}}{\partial H_1} + \frac{\partial \hat{m}_{13}}{\partial H_2} - \frac{\partial \hat{m}_{12}}{\partial H_3}\right)\dot{H}_1\dot{H}_2 + \frac{\partial V}{\partial H_3} \quad (23)$$

4. Establishment and simulation of virtual prototype

3.1 Establishment the virtual prototype

As a simulation scheme of prototype design, simulation technology greatly saves the time and cost of research and development, and improves the level of productivity. As a methodological tool, simulation technology provides designers with a wide range of perspectives and makes the error detection, parameter optimization, and mechanism analysis possible.

ADAMS is a software used to establish virtual prototype and analyze the static and dynamic mechanics of the system, but the modeling tool is relatively simple and not suitable for complex mechanism. SolidWorks is a very mature 3D graphics software, but it only has simple dynamic analysis and no control algorithm tools. Therefore, this paper establishes the 3D model of the 3-PRS ankle rehabilitation robot with SolidWorks, then the 3D model is imported into ADAMS for analysis.

To reduce the complexity of simulation of the 3-PRS ankle rehabilitation robot dynamics model, only the main characteristics required by the design of actual motion control law are retained. The following assumptions are adopted:

(1) All parts of the 3-PRS ankle rehabilitation robot can be used as rigid body, and the shape deformation is ignored.

(2) The friction, machining and assembly errors and environmental uncertainties of each joint in motion are ignored.

(3) There is a linear relationship between velocity and force.

The 3D model of the 3-PRS ankle rehabilitation robot is shown in Figure 1. The model is saved as a x_t format and imported into ADAMS to set up the simulation model. In order to get the simulation results close to the actual results, the quality, material, moment of inertia and other attributes of the imported virtual prototype are defined, and the corresponding constraints and system gravity are added.

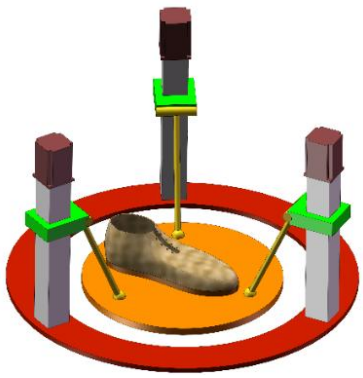

Figure 2: 3D model of the 3-PRS ankle rehabilitation robot

3.2 Kinematics calculation and simulation

The structural parameters of the 3-PRS ankle rehabilitation robot are shown in Table 1.

Table 1: Mechanism parameters of the 3-PRS ankle rehabilitation robot

Parameters	r / mm	R/ mm	L_i/ mm	m_N/ kg	m_L/ kg
Values	150	250	250	5.514	0.624
Parameters	m_h/kg	J_i/ kg mm^2	J_x/ kg mm^2	J_y/ kg mm^2	J_z/ kg mm^2
Values	0.22	1150	3110	3110	6200

(1) Inverse kinematics calculation

The motion rule of the moving platform is set as

$$\begin{cases} \alpha = 0.2\sin(\pi t) \\ \beta = 0.2\cos(\pi t) \\ z_t = 0 \end{cases} \tag{24}$$

where t is the duration of the exercise, and t is set to 4 seconds. The motion rules of the slider can be calculated by using the numerical calculation software, as shown in Figures 3 and 4.

(2) Inverse kinematics simulation

In ADAMS, the motion rule of the moving platform is set as Equation (24), the simulation time is set as 4 seconds, and the step size is 400 steps. The software simulates the motion rule of the slider as shown in Figures 5 and 6.

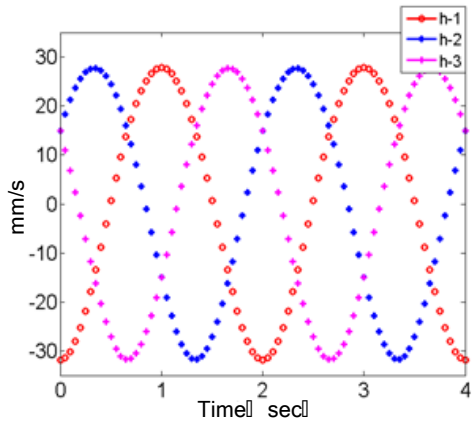

Figure 3: Calculated values of sliders displacement

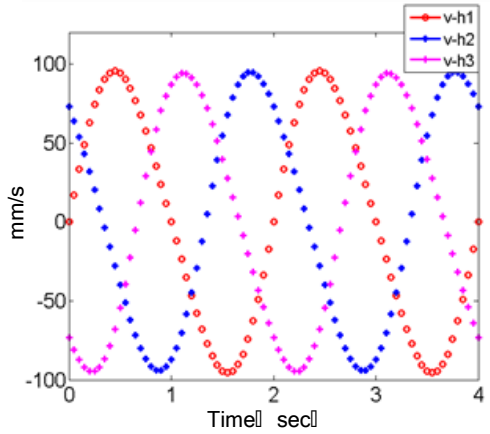

Figure 4: Calculated values of sliders velocity

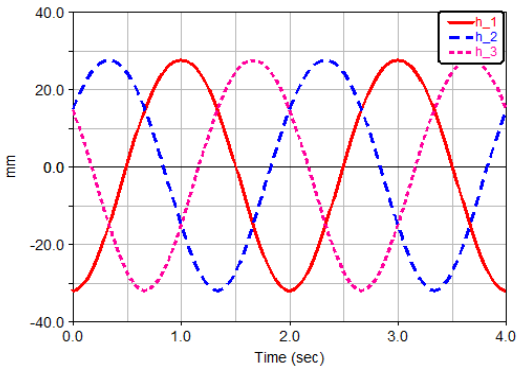

Figure 5: Simulation diagram of sliders displacement

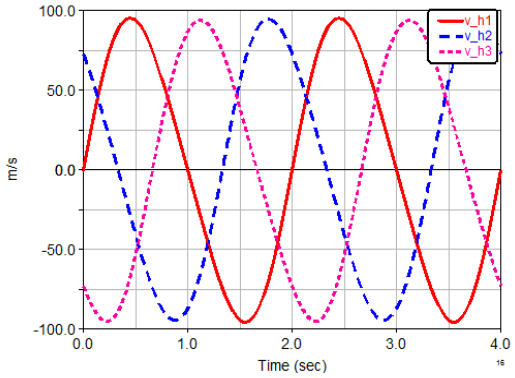

Figure 6: Simulation diagram of sliders velocity

By comparing the calculated value of the slider with that of the simulation, the motion rules of the two groups are basically the same, which indicates that the theory of inverse kinematics is reliable.

3.3 Dynamic calculation and simulation

(1) Inverse dynamics calculation

The motion trajectory of the moving platform is set as Equation (24). The driving force F_1, F_2 and F_3 of the three sliders can be calculated by solving the inverse dynamics equation with the help of numerical calculation software. The driving force changes with time as shown in Figure 7.

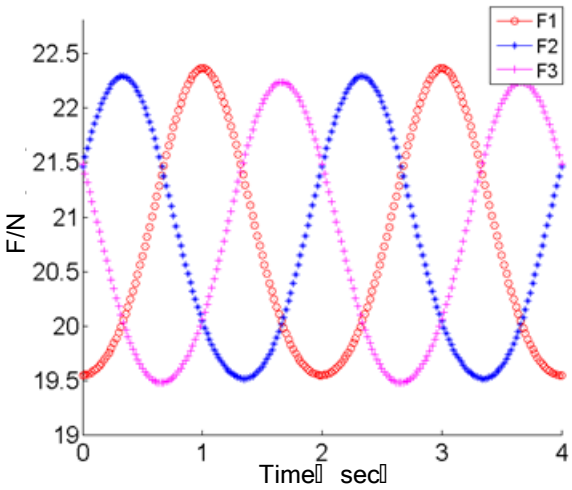

Figure 7: Numerical calculations of the driving force of sliders

(2) Inverse dynamics simulation

In ADAMS, 【Impose Motion(s)】 is clicked, and the motion parameters of the moving platform are set in the popup window, as shown in Table 2.

Table 2: Parameter settings table of 【Impose Motion(s)】

Dof	Tra X	Tra Y	Tra Z	Rot X	Rot Y	Rot Z
Type	Free	Free	0	0.2sin(πt)	0.2cos(πt)	Free

The simulation time is set as 4 seconds and the step size is set as 400 steps. The simulation results of

the slider driving force obtained by running the software is shown in Figure 8.

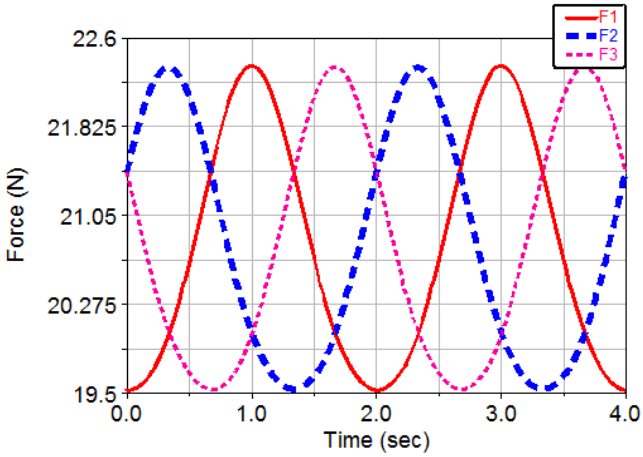

Figure 8: Simulation diagram of the pose of the moving platform

According to Figures 7 and 8, the theoretical derived value curve of inverse dynamics of the 3-PRS ankle rehabilitation robot is almost the same as the simulation value curve obtained by the software, which indicates that the dynamic theory research in the paper is reliable.

Conclusion

A virtual prototype model of the 3-PRS ankle rehabilitation robot is established by using dynamic analysis software. The dynamic model of the rehabilitation robot is established by Lagrange and the inverse dynamic equation is deduced. The kinematics and dynamics simulation of the robot is carried out by virtual prototype software, and the results are almost consistent with the theoretical analysis results, which verified the correctness of the theoretical research on the 3-PRS ankle rehabilitation robot, and laid a theoretical foundation for the future study on the control strategy of the 3-PRS ankle rehabilitation robot.

Reference

[1] C. Gosselin, L. T. Schreiber, Redundancy in parallel mechanisms: A review, Applied Mechanics Reviews, 2018, 70(1): 010802.

[2] Nakanishi H. Robot apparatus and parallel robot: U.S. Patent Application 15/757,369[P]. 2018-8-23.

[3] PAN G W, CHEN W L, WANG M. Review on the development of parallel mechanism technology for aircraft assembly, Journal of aviation, 2018, 40(1).

[4] LIU B Y, GAO F, JIANG H, et al. Attitude control algorithm of balanced rocker arm mobile robot, Journal of Beijing university of aeronautics and astronautics, 2018, 44(2):391-398.

[5] HU P H, LI S Y. Positive solution of parallel mechanism and its application in coordinate measuring machine, Optics and Precision Engineering, 2012, 20(4):782-788.

[6] Jamwal P K, Hussain S, Ghayesh M H, et al. Adaptive impedance control of parallel ankle rehabilitation robot, Journal of Dynamic Systems, Measurement, and Control, 2017, 139(11): 111006.

[7] Du Y, Li R, Li D, et al. An ankle rehabilitation robot based on 3-RRS spherical parallel mechanism, Advances in Mechanical Engineering, 2017, 9(8): 1687814017718112.

[8] SUN F W, ZHAO J W, CHEN G Q. A novel 3-PRS parallel mechanism and its workspace analysis are presented, Machine Tool & Hydraulics, 2017,45(23):19-25.

[9] Dai J S, Zhao T, Nester C. Sprained ankle physiotherapy-based mechanism synthesis and stiffness

analysis of a robotic rehabilitation device, Autonomous Robots, 2004, 16(2): 207-218.

[10] KANG J L, CHEN G Q, ZHAO J W. Analysis on workspace of 3-PRS mechanism based on montecarlo method, Journal of Henan Polytechnic University (Natural Science), 2014,33(4):478-481

[11] LI X F. Development of 3-PRS-XY series-parallel machine tool prototype, Henan Polytechnic University, 2015.

[12] Herrero S, Pinto C, Altuzarra O , et al. Analysis of the 2PRU-1PRS 3DOF parallel manipulator: kinematics, singularities and dynamics, Robotics and Computer-Integrated Manufacturing, 2018, 51:63-72.

[13] Elgolli H, Houidi A, Mlika A, et al. Analytical analysis of the dynamic of a spherical parallel manipulator, The International Journal of Advanced Manufacturing Technology, 2018,2:1-13.